*Highlights

Highlights

- Efficiency of hybrid coatings were assessed on calcarenite substrate by using several techniques
- Advantages and limitations of classic and innovative methods were highlighted
- **Al-Si-based product led to changes not advisable for calcarenite substrates**
- **Polyamidoamine-based product is more suitable for porous calcarenite consolidation**
- **Merits and limitations of the hydrophobic coating used in combination with consolidants were explored**

Graphical Abstract

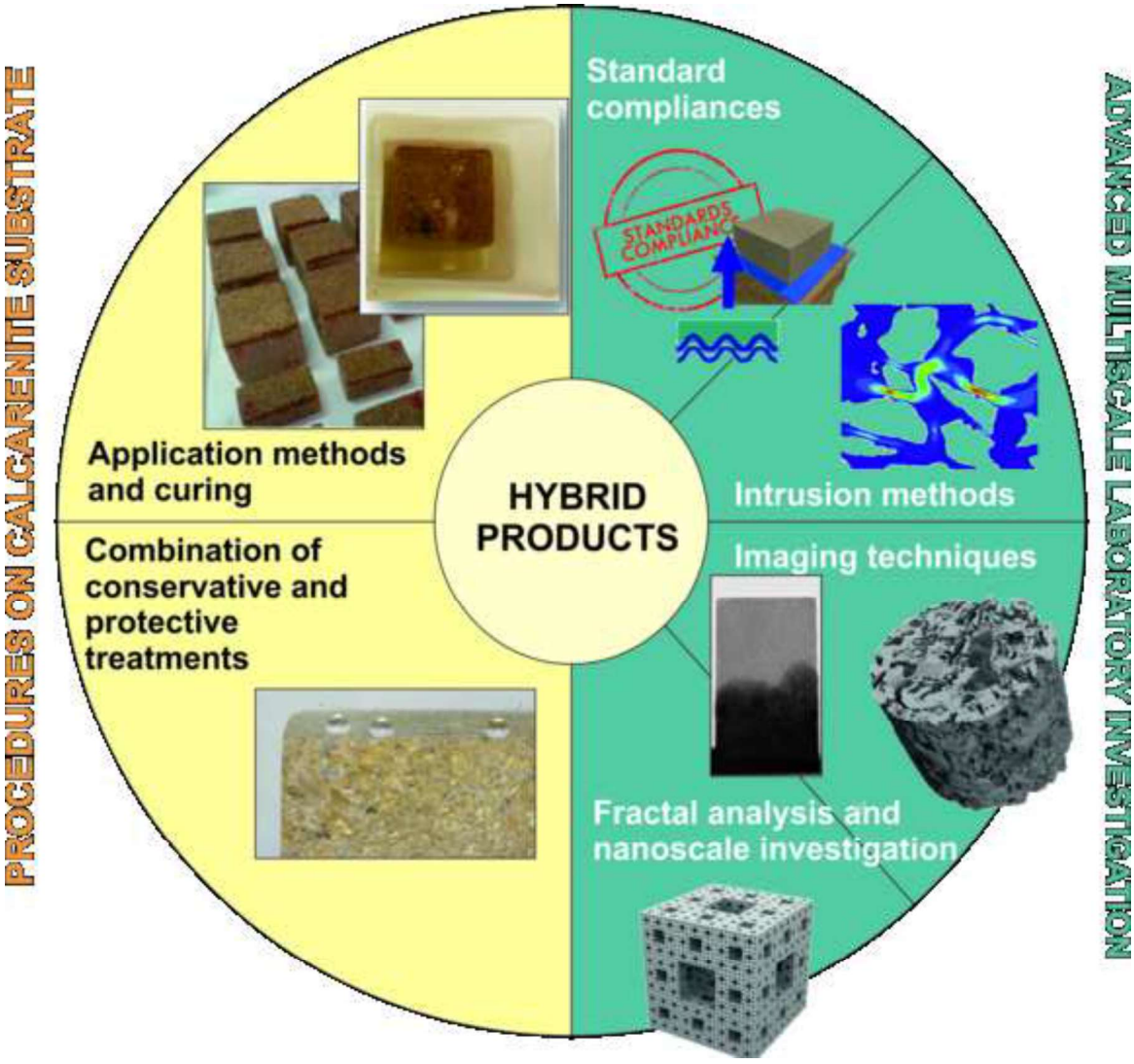

Efficiency assessment of hybrid coatings for natural building stones: advanced and multi-scale laboratory investigation

S. Raneri[1,2], G. Barone[1,*], P. Mazzoleni[1], I. Alfieri[3], L. Bergamonti[4], T. De Kock[5], V. Cnudde[5], P.P. Lottici[6], A. Lorenzi[3], G. Predieri[3], E. Rabot[7], J. Teixeira[7]

1 - University of Catania, Department of Biological, Geological and Environmental Sciences, C.so Italia 57, 95129 Catania, Italy

2 - University of Pisa, Department of Earth Science, Via Santa Maria 53, 53126, Pisa, Italy

3 - University of Parma, Department of Chemistry, Life Sciences and Environmental Sustainability, Parco Area delle Scienze 17/A, 43124 Parma, Italy

4 - University of Parma, Department of Engineering and Architecture, Parco Area delle Scienze 187/A, 43124 Parma, Italy

5 - Ghent University, Department of Geology, Krijgslaan 281/S8, B-9000, Ghent, Belgium

6 - University of Parma, Department of Mathematical, Physical and Computer Sciences, Parco Area delle Scienze 7/A, 43124 Parma, Italy

7 - Laboratoire Léon Brillouin (CNRS/CEA), CEA Saclay, F-91191, Gif-sur-Yvette, France

**Corresponding author: gbarone@unict.it*

Abstract

The efficiency of a hybrid patented consolidant (PAASi) and two commercially available hybrid coatings (a consolidant named AlSiX and a hydrophobic product named WS3) properly modified was assessed on a calcarenite substrate. Test routines based on standard recommendations were first applied to evaluate the performances of the consolidant and protective treatments, while the investigation of additional aspects such as penetration depth and interaction with the substrate was achieved by a multi-scale approach based on classic intrusion methods (mercury intrusion porosimetry) **and Drilling Resistance Measurement System (DRMS)**, combined with non-invasive imaging techniques (X-ray computed micro-tomography and neutron

radiography) and small angle neutron scattering (SANS). A distinct interaction of the products with the pore network of the stone was quantified in the range 0.007–200 μm. Their effects on capillary water absorption were also visualized with neutron imaging. The suitability of the products on the selected substrate was discussed, highlighting also how the applied routine can support conservation material studies. **The results indicated that the Al-Si-based product led to unwanted effects. Alternative application methods and/or curing procedures have to be explored to overtake these undesirable changes. On the contrary, the polyamidoamine-based product seemed to be more suitable for calcarenite substrates conservation. The performances of the hydrophobic coating, when used in combination with consolidants, were strictly influenced by the pre-consolidation of the substrate.**

Keywords: consolidants; **hydrophobic products;** stones; hybrid coatings; nanoparticles; efficiency

Highlights

- Efficiency of hybrid coatings were assessed on calcarenite substrate by using several techniques
- Advantages and limitations of classic and innovative methods were highlighted
- **Al-Si-based product led to changes not advisable for calcarenite substrates**
- **Polyamidoamine-based product is more suitable for porous calcarenite consolidation**
- **Merits and limitations of the hydrophobic coating used in combination with consolidants were explored**

Graphical abstract

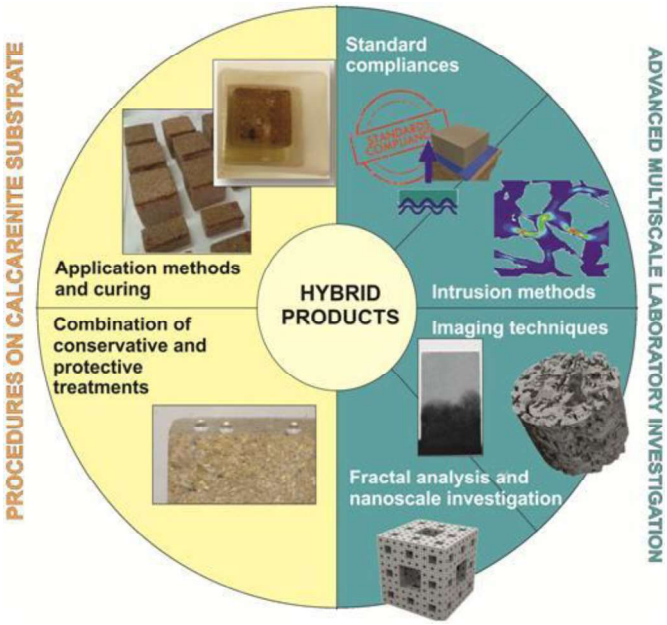

1. Introduction

One of the main difficulties in conservation field is the choice of suitable consolidants and protective treatments for stones, able to preserve masonry, compatible with the stone substrate of interest, and without any detrimental effect on its aesthetical properties. Protective products must preserve stones in their state of aging and prevent further decay. This generally means applying a coating to the stone surface. Consolidation, on the other hand, aims at stabilizing a friable material, while allowing weathering to take place at a natural rate as a result of natural processes.

The requirements for consolidant products mainly consist in a good stability, compatibility with the substrate [1,2], and a suitable penetration depth. A good consolidant should primarily reduce the rate of decay of the stone surface and improve its mechanical properties. In the ideal case, the treated stone should mimic sound stone in as many characteristics as possible, especially in terms of porosity, permeability, thermal expansion, water absorption and desorption, and color.

The main challenges in stone protection are related to the creation of a barrier against water penetration and the protection of the stone surface from pollutants and organic/inorganic particles deposition, while also ensuring the aesthetical compatibility with the substrate (i.e., color changes within acceptable ranges), the minimum alteration of the water vapor permeability and the reversibility of the treatment [3]. In this perspective, hydrophobic coatings [4], antifouling treatments [5] and self-cleaning nanoparticle-based protectives [6] are currently on the light of the research in stone preservation field [7].

Usually, tests based on standard recommendation procedures are **applied** to evaluate the efficiency of consolidants or protective products, mainly aiming at verifying their harmlessness with respect to the aspect of stones and their physical properties [8]. However, up to now, in spite of the huge literature in the field, no standard procedures and/or univocal methods for assessing **the efficiency of consolidants and protective products** are proposed [9]. Going **beyond** the classic approaches, usually using microscopy, micro-drilling, and ultrasound velocity tests [10], imaging techniques could add relevant information, as demonstrated by the recent applications in archaeological, geological, and industrial fields [11,12]. **Indeed**, neutron and X-ray imaging **techniques** allow inspect**ing** and **analyzing** numerous properties and processes, such as porosity,

79 water movement, degradation effects, amount and distribution of degradation products, or penetration depth
80 of protective and consolidant products [13–19].
81 In the case of consolidants, penetration depth and bonding **to the** substrate are the two main aspects to
82 investigate. Bonding ability greatly depends on both chemical composition of the product **used** (including
83 solvent and concentration) and the stone surface [10]. Usually, products having a composition **similar to**
84 **that** of **the** stone are preferred. **H**owever, this appears a non-exclusive requirement, **such** as in the case of
85 silicate-based networks largely employed in marble and limestone consolidation [20–22].
86 When a new product **is tested** on a new substrate, the first question is related to **the artificial aging of stones**
87 **to mimic the weathering of in situ conditions**. For limestones, salt weathering is a major cause of natural
88 degradation. However, **since** salts are usually difficult to remove and could influence the consolidati**on** test
89 results [23], laboratory tests are also performed on unweathered stones. Another aspect regards the
90 application method [24–26], where brushing is **sometime preferred because it ensures** a good product
91 application and a relatively controlled equilibrium between penetration and solvent evaporation. **Of course,**
92 **the testing of a new product requires preliminary tests aiming to identify the most suitable methods**
93 **and procedures** [10,27].
94 Among the new products synthesized for conservation of cultural heritage materials, hybrid **formulations**
95 **have recently been proposed for inorganic [28] and organic materials [29,30]. The term hybrid refers**
96 **to a product usually developed by sol-gel processes [31] and characterized by both the robustness of an**
97 **inorganic skeleton and the functional properties of an organic material [32]. With regards to**
98 **consolidants, the current researches have mainly explored the potential of TEOS-modified products by**
99 **using organic additives with the aim to overtake the limitations of negative long-term effects of**
100 **tetraethoxysilane [33–36] and to improve performances of consolidants, including water repellent**
101 **properties [37]. Among hybrid formulations, silicon-based products are becoming more and more**
102 **popular, due to the good processability and the stability of Si—C bonds during the formation of a**
103 **silica network, which allows the production of organic-modified inorganic networks in a single step.**
104 **Soft-matter chemistry applications are also focused on designing hybrid coatings having mainly the**
105 **scopes to improve repellency [38,39], performances [40] and durability of protective products against**
106 **aging [41].**

To evaluate the possible use of these new products for cultural heritage conservation, **and better understand how to tune hybrid formulations toward a better compatibility with highly porous and calcite-based stone substrates,** in this study, we tested a hybrid patented **product** (PAASi, [42]) and two commercially available hybrid coatings (a consolidant named AlSiX and a hydrophobic product named WS3) on a calcarenite substrate (named Sabucina Stone). **The synthesis of consolidants was designed to overtake possible limitations of such products. For the PAASi product, the amine would promote interaction with limestone substrate, while for the AlSiX product, the organic chains would contribute to limit shrinkage process during curing process.** The compositional and physical properties of **the** stone **selected** for consolidati**on** tests, especially its high porosity, give also the opportunity to inspect the potential use of the products **on** high**ly** porous materials, often difficult to consolidate [24]. To evaluate bonding and penetration ability of **the** products, consolidati**on** tests were performed on **an** unweathered treated substrate, to avoid **the** difficulties related to **the** artificial weathering, such as **the** presence of salts and no proper desalinization. **Efficiency** and suitability of the products were firstly evaluated by monitoring absorption, desorption, color, **resistance to** artificial weathering, and pore structure changes. **T**hus, non-invasive investigation**s** by using X-ray and neutron sources were performed to visualize products inside stones and the **possible** pore network modification. Finally, additional structural information on the employed products was obtained with small angle neutron scattering (SANS) technique.

Consolidants were applied by **immersion to have maximum penetration depth and fully impregnated specimens. In view of combining both consolidation and a protective application, hydrophobic coating was therefore applied by** brushing **the treated specimens. Finally**, for structural studies by SANS, **samples were treated by both brushing and** immersion, to evaluate the possible influence of the method in small scale structural changes **and penetration in nano-sized pores**.

2. Materials and methods

2.1 Materials

2.1.1 Natural building stone

A coarse grained calcarenite, named Sabucina stone, employed in Sicilian monuments as building and replace material was selected for this study [43]. **The stone is a biosparite with grainstone/packstone**

texture, mainly composed by calcium carbonate, along with small quantities of dolomite. It exhibits a porosity of ~27%, with a total pore volume of 0.14 cm^3 g^{-1} and a modal pore radius of about 8.5 μm. Further details on the petrography, mineralogy, chemical composition, petrophysics, and porosimetry of this lithotype are provided in Barone et al. [44].

For this study, **225** samples were obtained from a unique freshly quarried block sampled at Sabucina Mountain (Caltanissetta, Sicily), varying in dimension and shape in accordance with the requirements of the applied methods and recommendations **(see Table 1)**.

2.1.2 Hybrid products

Two different hybrid inorganic-organic consolidants were synthesized and tested on Sabucina stones, namely (i) a polyamidoamine-based product with siloxane functionality (PAASi), and (ii) a silicon alkoxide with epoxy functional group and aluminum oxide (AlSiX). The schematic chemical structure of both products is shown in Figure 1.

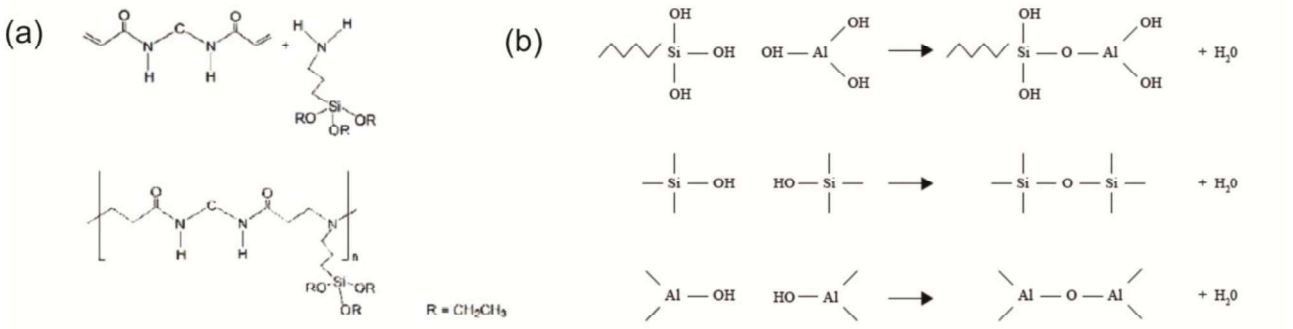

Figure 1. Pictorial sketch showing (a) the reaction producing PAASi and (b) the main reactions involved in the sol formation of AlSiX.

The hybrid product PAASi is a patented wood protective material [42], modified for its application on stone substrates. The product was synthesized by the Michael-type reaction, adding 3-aminopropyltriethoxysilane (APTES) to N-N'methylenebisacrylamide (MBA). In detail, in a flask placed in a thermostatic bath at 30°C, 5×10^{-2} mol of MBA were dissolved in 190 mL of deionized water and the solution was stirred for 20 min. After complete solubilization of MBA in water, 5×10^{-2} mol of APTES, mixed in 10 mL of ethanol were added. The obtained solution was vigorously stirred in the thermostatic bath at 40°C for 2 h**. A 0.25 M sol**

was finally obtained. The inorganic group inside the stone can polymerize in situ by hydrolysis and condensation reaction, forming a 3-D network.

The hybrid sol AlSiX is based on an Al-O-Si network functionalized with organic chains and epoxy groups, having the role of reducing the brittleness of the inorganic structure. The sol was synthesized by sol-gel process starting from a solution of aluminum and silicon alkoxides in propan-2-ol. The stoichiometric amount of water acidified with HCl was added to hydrolyze the precursors. The stirring was prolonged until a completely transparent sol was obtained. The sol was then diluted adding water (alcohol/water volumetric ratio = 1:2). The final concentrations of aluminum and silicon were 0.33 M and 0.66 M, respectively.

For the treatment of the studied substrates, cubic samples of Sabucina stone ($4 \times 4 \times 4$ cm^3) were preliminary washed in distilled water and dried at 60°C to constant mass [45]. Samples were thus plunged into PAASi and AlSiX sols in sealed containers for 1 h and dried at 60°C to constant mass. Samples were cured 1 month at room temperature (RT) condition.

The average quantity of applied products was calculated as weight percent gain (WPG%): $WPG\,\% = 100 \cdot [(M_t - M_0)/M_0]$, with M_0, the mass of dry sample before the product application, and M_t, the mass of dry sample after product application. The calculated quantities were 1.9% ± 0.1 WPG% for AlSiX and 1.4% ± 0.3 WPG% for PAASi.

2.1.3 Hydrophobic coating

A colloidal silica with fluorinated groups named WS3 was tested as coating on Sabucina stones treated with PAASi and AlSiX, to verify its hydrophobic efficiency and suitability on treated calcarenite substrates.

The treatment was prepared by mixing -O-Si-O-Si(R_f)-O- siloxane chains (with R_f, the fluorinated groups) and colloidal silica: the fluorinated groups provide the hydrophobic functions, while the colloidal nanoparticles enhance the water repellency by creating a suitable surface texture. The silica nanoparticles size was about 10 nm, whereas the resulting siloxane aggregates were micrometric in size.

For this study, WS3 was applied by brushing on cubic samples after the application of PAASi and AlSiX. The average quantity of product applied was 0.7 ± 0.1 g m^{-2}, calculated as the difference between the weight of dry specimens after and before the treatment (dry matter).

2.2 Characterization methods

2.2.1 Physical and mechanical tests

A protocol based on standard NORMAL and UNI EN tests was applied in order to verify the compatibility of the studied products and their suitability on calcarenite substrates. In detail, comparative colorimetric, physical (water absorption, drying and salt crystallization resistance), and mechanical (**microdrilling resistance**) tests were performed on untreated and treated samples.

Firstly, to evaluate the hydrophobic characteristics of the coating, contact angle measurements were performed on samples after the application of WS3 according to UNI 11207:2007 [46].

Color difference between treated and untreated samples **(ΔE^*)** was evaluated according to UNI EN 15886:2010 [47]. The absorption coefficient by capillarity AC (g cm^{-2} s$^{-0.5}$) was evaluated according to the UNI EN 15801:2010 recommendation [48] on three cubic samples for each treatment (with edges of 4 cm) by applying the following time intervals: 5 min, 10 min, 20 min, 30 min, 60 min, 4 h, 6 h and 24 h, […], 7 days). Water absorption by total immersion was evaluated following the NORMAL 7/81 recommendation [49], that allows calculating the imbibition coefficient CI (%). **This** test was performed on fifteen samples for each treatment (time intervals: 5 min, 10 min, 20 min, 30 min, 60 min, 4 h, 6 h and 24 h, […], 72 h). **The drying index DI was determined following the NORMAL 29/88 recommendation** [50]. Saturated samples from the previous NORMAL 7/81 were used for this test. The resistance to aging by soluble salts was determined according to the UNI EN 12370:2001 test [51], performed on 15 cubic samples for each treatment (4 × 4 × 4 cm^3).

Following the UNI EN 15803:2010 norms [52], the water vapor permeability tests were performed on treated and untreated stone samples 4x4x1 cm^3 , mounted on of PVC containers, partly filled with water; the sealed containers kept in a climatic chamber (R.H. 25% and $T = 25 \pm 0.5$°C), were weighted every 24 h until the mass change per unit time were constant (i.e. constant value of vapor flow through the stone). The effect of the treatments on the water vapor permeability was quantified by $RVP\% = \frac{m_{uv} - m_{tv}}{m_{uv}} \cdot 100$, called reduction of vapor permeability, with m_{uv} = mass of water vapor penetrating untreated stone and m_{tv}= mass of water vapor penetrating treated stone, measured in the steady state [53].

Microdrilling resistance was determined by drilling resistance measurement system (DRMS) [54] **on consolidated specimens cured several months. For this study, 3 mm diameter Widia drill bit was used, with a rotation speed of 800 rpm and a penetration rate of 10 mm min^{-1}. For each treated specimen and for a reference untreated one, four holes were drilled over 5 mm in depth from the surface. The average force as a function of depth was reported.**

2.2.2 Mercury intrusion porosimetry (MIP)

Mercury intrusion porosimetry (MIP) measurements were performed by using a Thermoquest Pascal system (coupled 240 and 140 units) to explore a pore radii range from 0.0074 to 116 μm. Average data were assessed on measurements performed on three small specimens similar in dimension and shape **(cubes of ~1 cm^3) sampled at the surface of cubic samples coated with AlSiX and PAASi.** Data were processed by using the SOL.I.D (Solver of Intrusion Data) software.

2.2.3 X-ray computed micro-tomography (μCT)

μCT scans were performed at the Centre for X-ray Tomography (UGCT, Ghent University, Belgium) [55]. Cylindrical samples with a diameter of 7 mm were scanned before and after the treatment with AlSiX and PAASi **at the stone surface**. An overall of 1201 projections were acquired **over an angle of 360°** with a **source-detector distance** of 1165 mm and a **source-object distance** of 22 mm, resulting in a voxel size of 7.5 μm. **A voltage of** 120 kV, **a power of** 10 W, and **a tube current of** 83 μA were imposed. **Additionally**, **a** beam hardening effect was **reduced** by using an Al-filter (1 mm). Only objects with a minimum of 3 voxels were retained in reconstruction analysis. Because the consolidation products tend to have attenuations for X-rays similar to those of the minerals of the stone samples, Ag^+ ions (from $AgNO_3$) were added to the studied products as tracer. Before the application on Sabucina stones, $AgNO_3$ was directly dissolved in the sols by vigorous stirring (molar ratio PAASi monomer/Ag^+ = 2500:1 and Si(AlSiX)/Ag^+ = 2500:1). μCT data were reconstructed with the Octopus Reconstruction software [56], while 3-D visualization and quantification were obtained by using VGStudio MAX (Volume Graphics) and Octopus Analysis (former Morpho+) [57], respectively. Only objects of a minimum of 3 voxels were retained in the analysis.

2.2.4 Neutron radiography

Neutron images were acquired on 15 samples ($2 \times 2 \times 4$ cm^3) of the studied stone with either consolidant or water repellent products, with the aim of (i) visualizing the penetration depth of the selected products after polymerization and (ii) monitoring the water absorption process by capillarity, to evaluate the possible modification of the physical properties of the stones. Neutron **radiographs** were acquired at **the** IMAGINE beamline of the Laboratoire Léon Brillouin (LLB, Saclay, France), using a neutron flux of 2×10^7 neutrons s^{-1} cm^{-2} (cold neutrons with wavelength in the range 3–20 Å), a *L*/*D* ratio of 400 and a sCMOS camera (Andor) coupled with a lithium scintillator of 100 µm thickness. **This set-**up allowed a spatial resolution of about 250 µm.

Dark field and open beam images were firstly acquired for further corrections. **S**amples were scanned in an aluminum container and a reference image in dry state was acquired. To monitor capillary uptake, water was manually added by filling the container with 3 mm of water. **A**fter the addition, scans were acquired every 40 s until saturation **with an exposure time of 40 s. T**he duration of the **whole** experiment was about 20 min.

Image analysis was performed by using **the** ImageJ software [58] on **radiographs** corrected and normalized by dark field and open beam images. Water content distribution was quantified according to Kim et al. [59]. Moreover, **the** sorptivity parameter (*B*) was experimentally determined from the radiographs, according to Philip [60] .

2.2.5 Small angle neutron scattering (SANS)

Small angle neutron scattering measurements were performed on the PAXY instrument (cold neutron guide G2) at the ORPHEE reactor of the Laboratoire Léon Brillouin (LLB, Saclay, France). Neutrons **were** monochromatized by a mechanical selector and collimated by two slits 5 m far apart. **S**cattered neutrons **were** collected by a 2-D BF_3 detector consisting in 128 × 128 cells, **each** of them measuring 5×5 mm^2. **T**wo different set-ups were used to explore different Q ranges: for large Q (from 3.2×10^{-2} to 0.28 Å^{-1}), **the wavelength** $\lambda = 6$ Å and **the sample-detector distance** = 1 m, **whereas** for small Q (from 4×10^{-3} to 3.6×10^{-2} Å^{-1}), $\lambda = 8.5$ Å and **the sample-detector distance** = 5 m.

In order to minimize multiple scattering effects, measurements were performed on thin sections of treated stone, with thickness < 1 mm. **S**lices were treated with AlSiX and PAASi by different **application** methods,

i.e., by brushing and by immersion under vacuum to investigate the possible variation in pore surface-air interface due to the product deposition. No appreciable neutron activation of the samples was found after the experiment.

The two-dimensional intensity distributions were corrected for the background and **normalized** by measuring the incident beam intensity, transmission, and sample thickness. One-dimensional data were obtained by integrating the normalized two-dimensional intensities with respect to the azimuthal angle. At large Q, the constant asymptotic incoherent scattering of the hydrogen atoms present in the samples was subtracted. The coherent scattering I(Q) **is** expressed in cm^{-1} and corresponds to a differential coherent cross-section per unit volume of the samples. Starting from the I(Q) distributions, roughness of the pores surface in term**s** of surface fractal dimension D_s [61], were obtained for untreated and treated samples according to the following equation:

$$I(Q) \propto Q^{-(6-D_S)}$$

3. Results and Discussion

3.1 Physical and mechanical tests

3.1.1 Static contact angle

The test confirmed the hydrophobic behavior of the WS3 product, with an average measured contact angle of 130° ± 2°.

3.1.2 Colorimetric tests

In **Table 2**, the total color difference ΔE^* between treated and untreated stone samples, calculated on the basis of the measured colorimetric parameters a^*, b^*, and L^* are reported (approximated to the integer).

As reported in the literature [62]**,** a conservative treatment should not **lead to a total color change** greater than 5. **The AlSiX product clearly led to strong chromatic changes, especially when used in association with the hydrophobic coating. This could be related to the presence of aluminum bonded with the silica network. Conversely, the application of PAASi had acceptable chromatic changes, even if the presence of hydrophobic coating led to higher ΔE^*.**

298 *3.1.3 Comparative water absorption-desorption and accelerated aging test*

299 The average capillary absorption curves assessed on three samples for each treatment (*i.e.,* untreated, PAASi,
300 PAASi + WS3, AlSiX, AlSiX + WS3) are shown in Figure 2a, and the absorption coefficients AC, evaluated
301 as the slope of the line fitted to the evolution of Q_i as function of $t^{0.5}$ in the first 30 min are reported in Table
302 **3**. The samples treated with PAASi showed slightly lower capillary absorption **as** compared to the untreated
303 stones, with a low increase of the absorption coefficient in the first 30 min of the test. In samples treated with
304 AlSiX, the capillary absorption decreased **as** compared to the untreated stones, especially during the first 30
305 min of **water** absorption. Finally, the presence of the hydrophobic coating WS3 led to a reduction of the
306 water absorption by capillarity, with a decrease of AC from 0.03 g cm^{-2} $s^{-0.5}$ to 0.01 g cm^{-2} $s^{-0.5}$. The amount
307 of water absorbed by capillarity at the transition from the first to the second stage of the capillary absorption
308 curves (***i.e.***, after 4 h) can be used to evaluate the changes in porosity accessible to water before and after the
309 treatments [63]. On the basis of the obtained data, it is possible to estimate the following effective porosity:
310 ~21% in untreated stone, ~19% and ~14% in samples treated with PAASi and AlSiX, respectively. A more
311 important decrease (up to ~13%) can be observed for samples coated also with the hydrophobic **product**
312 WS3. These results indicate that the two consolidants reduce**d** the effective porosity **of** about 2% (PAASi)
313 and 7% (AlSiX). Of course, in the case of samples treated also with hydrophobic product, the calculated
314 porosity has to be carefully considered, as its drastic reduction is plausibly attributable to the coating **at** the
315 **stone** surface.

316 For the total immersion test, the average curves calculated on 15 samples for each treatment are reported in
317 Figure 2b. The **imbibition coefficient** CI after 72 h (Table **3**) highlight**s** a slight decrease (of about 1%) of
318 the water imbibition for samples treated with both consolidants, whether associated or not with WS3. This
319 indicates that the total porosity **was** not strongly modified by the treatments, while more relevant
320 modifications occurred in **the** pore structure arrangement, **mainly affecting** capillary water absorption. **To**
321 **summarize, treated samples have a lower absorption of water by capillarity and total immersion,**
322 **proving the deposition of the products in pores and/or pore throats.**

323 The use of both consolidants and hydrophobic treatment also influenced the drying properties of the studied
324 stone, as suggested by the increase of the dry index DI for samples treated with consolidants and coated or
325 not with WS3 (Figure 2c and **Table 3**). The treatments modified the overall drying rate of Sabucina stone,

affecting particularly the second phase of the drying process, which is strongly governed by vapor diffusion. **Indeed**, the critical moisture content **was** higher for **the** treated samples, in **agreement** with the observed decrease in the capillary coefficient.

The results on the reduction of the vapor permeability $RVP\%$, calculated after a 14 days test are reported in Figure 3. The stone samples treated with ALSiX and PAASi consolidants show %RPV values in the range 4-10%, below the acceptable threshold of 20% [64]**. On the contrary, for the combined use of consolidants and hydrophobic treatment, the reduction of vapor permeability is significantly higher (40-45%); actually, it is not unusual that hydrophobic films determine strong water permeability reduction when used onto porous substrates** [65]**.**

As regards aging tests (Figure 2d)**,** PAASi **seemed** to improve the resistance to salt crystallization, with a decrease of the mass loss after 15 cycles (**Table 3**), from −11.1% (untreated samples) to −6.6%. It is noteworthy that the presence of WS3 slightly increase**d** the mass loss, from −11.1% to −12.7%. For AlSiX, even if the product resulted in lower absorption **properties**, it was responsible for a slight decrease of the durability of the studied material: an increase of the mass loss after 15 cycles was observed for treatments with AlSiX and AlSiX + WS3. It is possible to assume that the reduced capillary transport might **have** cause**d** a faster shift towards phase 2 in drying at higher moisture content (and thus lower salt concentrations), so that supersaturation **was** reached with a drying front within the stone, **leading to an increase in** mass loss.

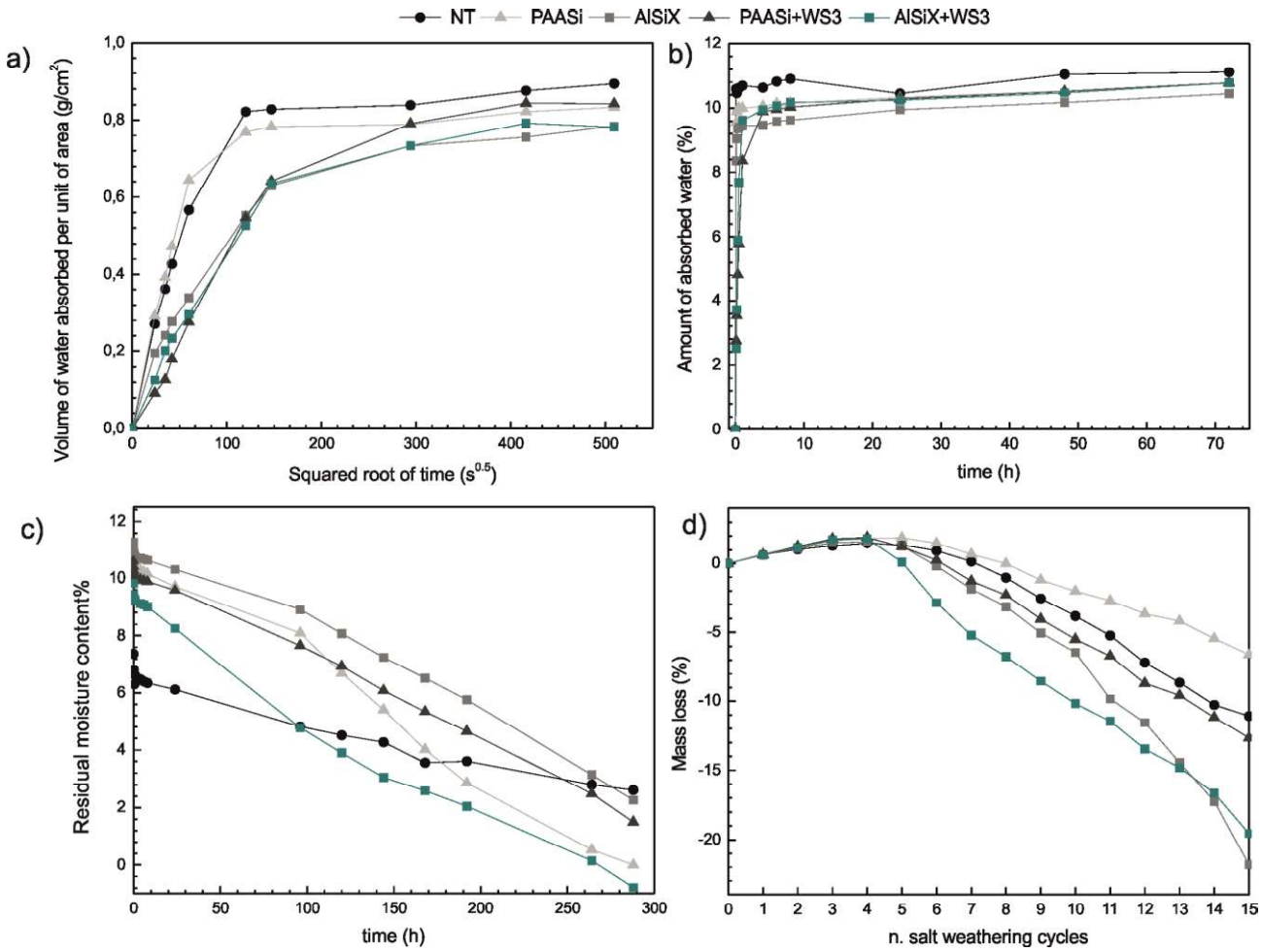

345

346 *Figure 2. Water absorption by (a) capillarity and (b) total immersion, (c) drying and (d) durability tests performed on untreated*
347 *stones (NT) and stones treated with both consolidants (PAASi and AlSiX) and hydrophobic (WS3) products.*
348

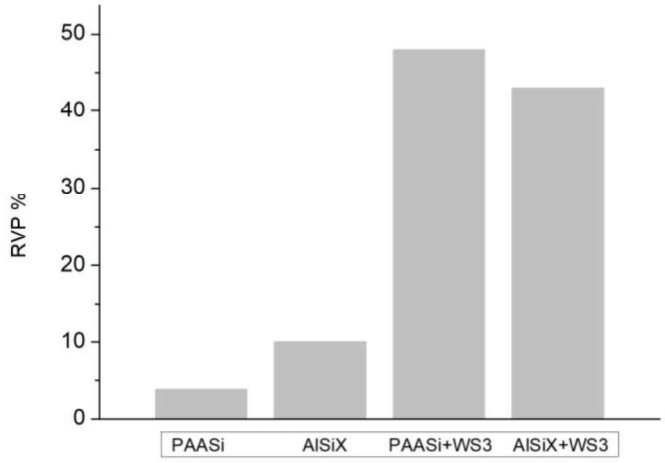

349

350 *Figure 3. Reduction of vapor permeability RVP% for different treatments.*
351

3.1.4 Drilling resistance

Fig. 4 shows the drilling resistance graphs obtained by drilling resistance measurements on untreated and treated specimens cured in laboratory during several months.

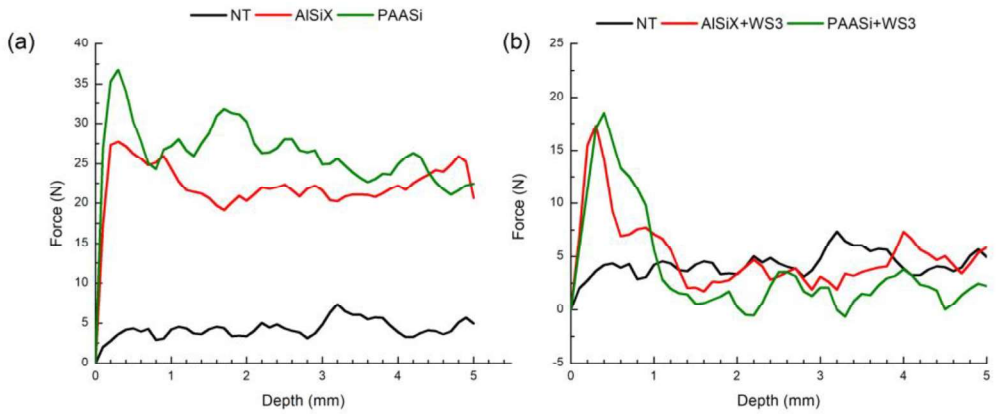

Figure 4. Drilling resistance on Sabucina stones treated with (a) consolidants (AlSiX and PAASi) and (b) consolidants in combination with hydrophobic product (WS3).

The curve describing the behavior of the untreated stone (black line) highlights a natural variation in strength, probably related to the texture of the stone. Overall, the drilling resistance of the stone was quite low (about 4–6 N).

The two consolidants promoted both an increase in strength, well pronounced in the first 1–2 mm. In combination with the hydrophobic product, the strengthening effect was strictly limited to the first millimeter. Potentially, this behavior could be ascribed to the different long-term curing dynamic, *i.e.*, influence of the hydrophobic layer on moisture transfer during polymerization.

3.2 MIP

Table 4 reports pore structure parameters obtained on untreated samples and samples treated with AlSiX and PAASi. In **agreement** with **the** results **of the** absorption tests, products **did** not greatly modify the total porosity, **but** mainly **affected** the pore structure arrangement of the stone. **For AlSiX**, a strong shift of the average pore radius and of the median and modal pore sizes can be observed, from 0.14 µm to 0.22 µm, from 8.56 µm to 12.55 µm**, and from 2.25 µm to 4.21 µm,** respectively. The ranges of these variations are

adequately expressed by the cumulative volume intrusion and pore size distribution curves (Figure 5a), **suggesting the impregnation of pore larger than 5 µm**.

For the PAASi treatment, the small differences in the porosimetric parameters could only be related to the already attested variability of the stone**, even if some variations can be observed in the cumulative volume intruded and pore size distribution curves (Figure 5b).**

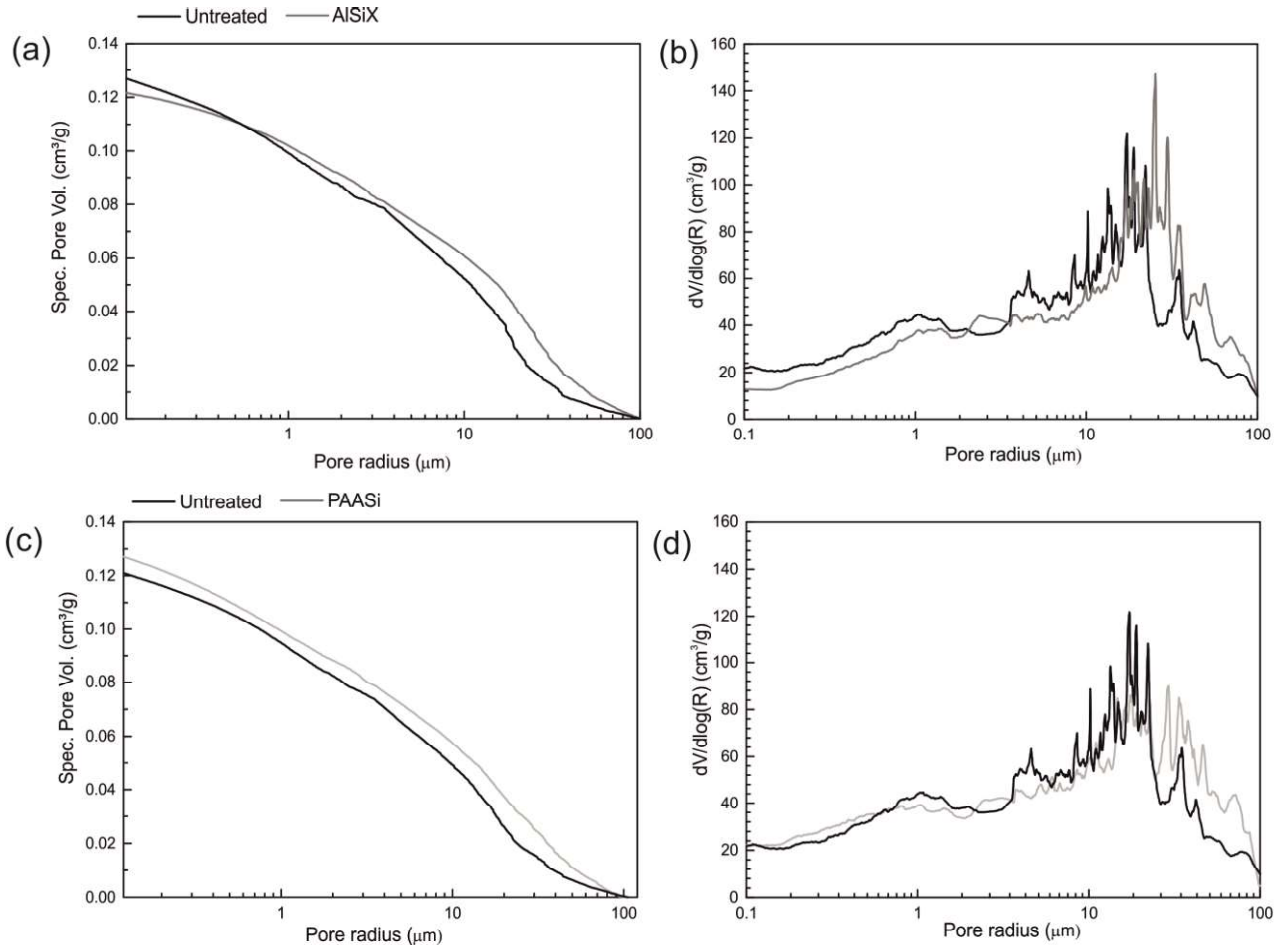

Figure 5. Pore size distributions represented as (a, c) cumulative or (b, d) differential pore volumes, measured on untreated samples (black) and samples treated with (a, b) AlSiX and (c, d) PAASi consolidants (gray).

3.3 µCT

In order to better visualize the distribution of the studied consolidants inside the pore space of the stone, scans were performed on small cylindrical samples before and after the application of the products. µCT scans were obtained by subtracting measurements collected on untreated and treated samples. The untreated stone had a resolved porosity of about 11.7% (with open and closed porosity values of 10.1% and 1.6%,

respectively), and pore distribution described by equivalent diameter (ED) and maximum opening (MO) ranging from 7.5 µm to 967.5 µm and from 7.5 µm to 372.5 µm, respectively (see also [66]).

After the application of the AlSiX product, the resolved porosity **of the whole sample** decreased by 2%. From an inspection of ED and MO distributions (Figure **6a and** b), it is possible to conclude that **AlSiX** impregnated pores exhibiting ED values from 7.5 to 500 µm and pores with MO values between 7.5 and **150** µm. Pores having ED > 500 µm and MO > 150 µm **were** not **affected** by the treatment. The 3-D image reconstructions presented in Figure **5**c allow visualizing the distribution of **AlSiX** into the pore network of the stone (in red). Of course, due to **the** voxel resolution, only pores with ED > 7.5 µm can be considered. **Therefore**, it is possible that pores with ED < 7.5 µm also contain consolidant.

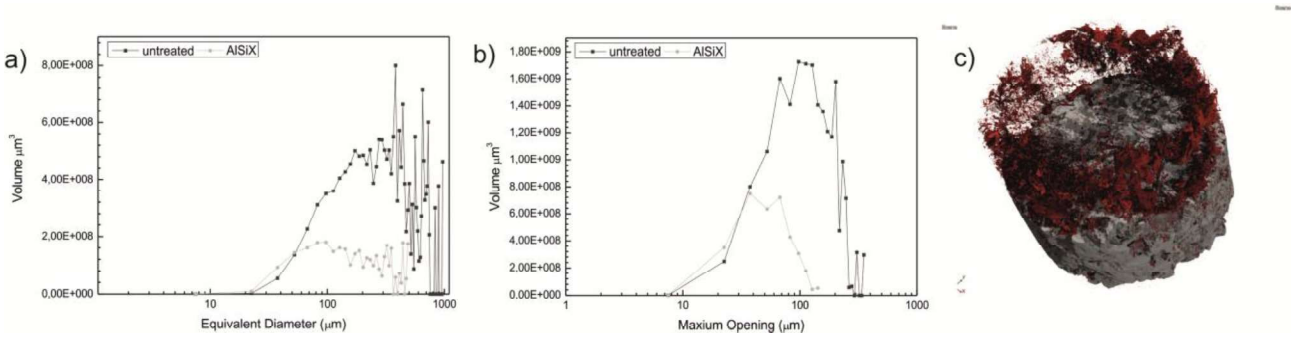

Figure 6. Pore volume as function of (a) the equivalent diameter and (b) maximum opening for AlSiX treatment (step intervals 2 voxels, i.e., 15 µm). (c) 3-D visualization of the bulk material (gray) and distribution of AlSiX (red). The sample diameter is approximately 7 mm.

Before PAASi application, the resolved porosity of the untreated samples was about 12.3% (with open and closed porosity values of 10.8% and 1.5%, respectively), and the pore network was characterized by pores ranging from 7.5 µm to 1220 µm in ED and **from** 7.5 µm to 400 µm in MO. A reduction of 0.8% of the resolved porosity **of the whole sample** was observed after **PAASi** application, suggesting a very poor impregnation ability of PAASi. This behavior was confirmed by the ED and MO distributions relative to pores filled by the consolidant (Figure **7a and** b), indicating that only a limited range of pores (*i.e.,* ED ~40–300 µm and MO < ~70 µm) was involved. This low impregnation ability is also visible in the 3-D representation (Figure **7c**).

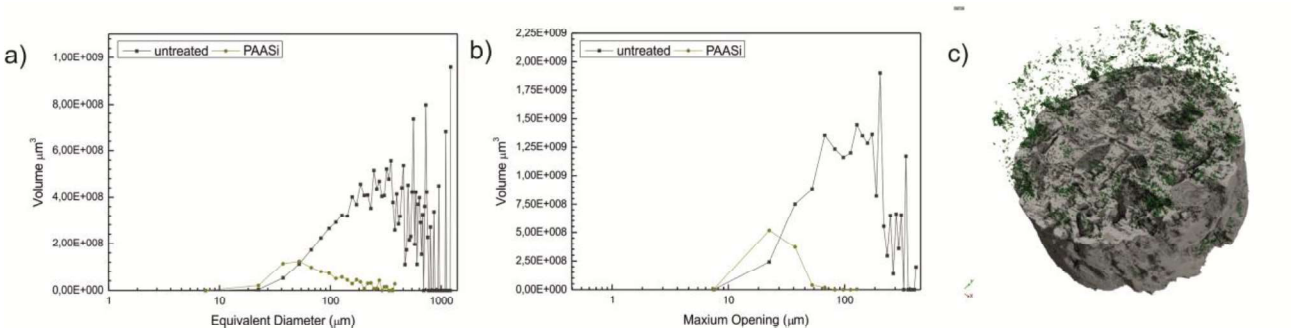

Figure 7. Pore volume as function of (a) ***the*** *equivalent diameter and (b) maximum opening for PAASi treatment (step intervals 2 voxels, i.e., 15 µm). (c) 3-D visualization of the bulk material (gray) and distribution of PAASi (green).The sample diameter is approximately 7 mm.*

By comparing the behavior of the two different studied products (Figure **8**), it is possible to conclude that in the case of PAASi, the product mainly impregnated pores with ED in the range from 50 to 100 µm and MO in the range from 7.5 to 50 µm, whereas in the case of AlSiX, the product involved larger pore ranges (ED between 100 and 500 µm, MO between 50 and 150 µm). It indicates a different interaction of the products with the pore network of the stone, with **PAASi** penetrating into finer pores than AlSiX.

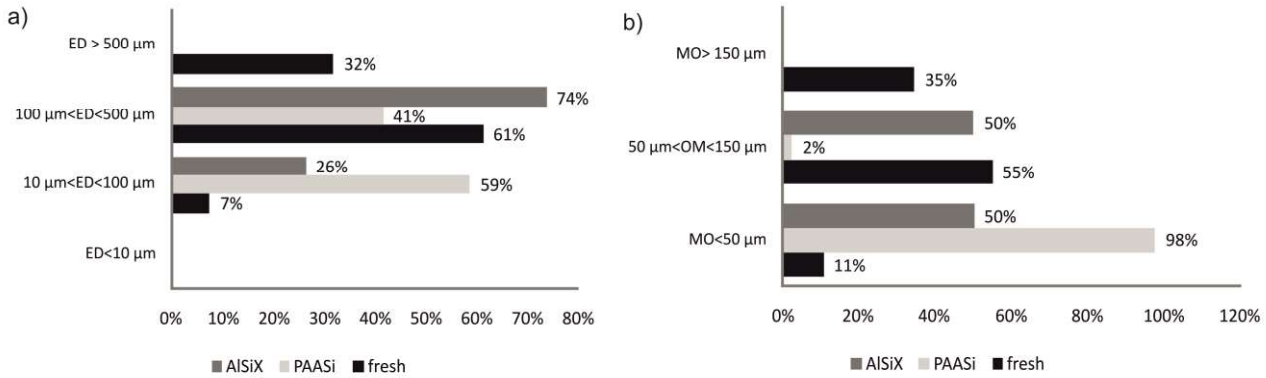

Figure 8. Comparison of (a) the equivalent diameter (ED) and (b) maximum opening (MO) classes impregnated with consolidants (AlSiX and PAASi).

3.4 Neutron radiography

Neutron radiographs acquired for treated Sabucina stone samples are shown in Figure **9**. In the sample treated with AlSiX, the radiograph shows the presence of product inside the sample, resulting in an increased attenuation of the neutron beam close to the sample edges. **The product may be homogeneously distributed up to a penetration depth of 2–3 mm, in agreement with microdrilling results. A lower amount of product may reach 5 mm depth**. Such a behavior can also be observed in the case of the combined use of AlSiX and water repellent WS3.

In the case of samples treated with PAASi, the presence of consolidant is hard to detect in the radiographs**,** **due to a low interaction between the neutron beam and the product.** Similar observations can be made for the combination PAASi + WS3. **Nevertheless, information about the penetration depth are available from drilling resistance, attesting a relevant increase in strength up to a depth of a few millimeters.** The water repellent product cannot be distinguished, because its thickness may be too small for a good contrast between untreated and treated areas. Of course, it has to be taken into account that the two products consist in chemical components differently detectable by neutrons, so that PAASi has credibly a lower attenuation coefficient than AlSiX.

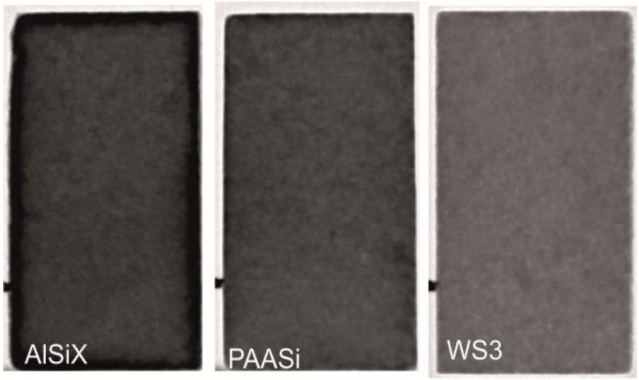

Figure 9. Neutron radiographs of samples treated with consolidant (AlSiX and PAASi) and water repellent (WS3) products.

Water movement by capillarity was monitored over time through neutron radiography. Radiographs were acquired at 5, 10, 15, and 20 min after the addition of water at the bottom of the samples, for a reference untreated sample and for samples representative of different treatments. The 2-D distribution of water and the wetting front advancement can be easily visualized. In Figure **10**, the profiles of intensity values at selected time steps obtained from the central vertical column of pixels in the normalized transmission images are reported. The wetting front position **was** determined as the inflection point of the profile, indicating the transition between low intensity values (saturation) and higher intensity values (dry conditions).

The wetting front positions were related to time and the sorptivity parameters (*B*) were determined by using linear regressions. The **wetting front** migrating inside the treated samples was slightly slowed down by the presence of the products (Table **5**), even if during the first minutes of contact with water, a faster advancement of the wetting front position was observed.

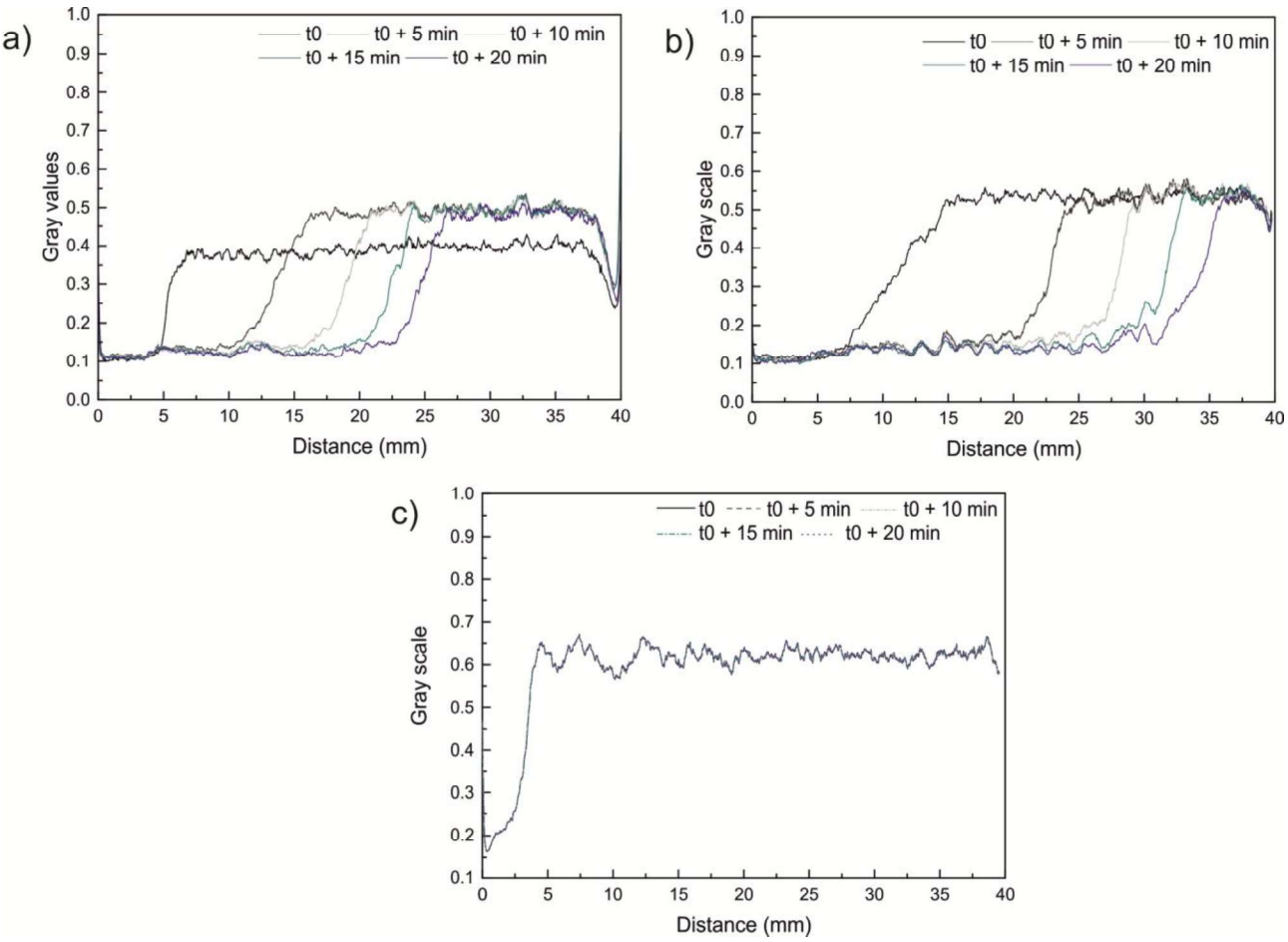

*Figure **10**. Profiles of intensity values of samples treated with (a) AlSiX and (b) PAASi consolidants, and (c) hydrophobic product WS 3at selected time steps during capillary water uptake. The 0 reference distance is the bottom of the samples.*

In order to quantify the water distribution and to better understand the water absorption process in treated samples, the thickness of water crossed by the neutron beam as a function of time was estimated. Examples of contour plots of the water content distribution (WC%) estimated from the neutron radiographs at 5, 10, 15, and 20 min after the addition of water are shown in Figure **11**. In the case of the AlSiX treatment, WC% was lower than in the untreated samples (always < 2%). Water penetrated preferentially through areas not impregnated by the consolidant, as can be seen by the lower WC% close to the lateral edges. On the contrary, for the PAASi treatment, an increase of the water absorbed was observed (WC% > 2.5–3%). Finally, the performances of hydrophobic treatments (used both alone and in combination with consolidant) are clearly evidenced: the contour plots show that no water invaded the samples during the first minutes of contact with water. The layer visible at the bottom of the radiographs has to be related to the set-up reservoir. **Overall, these results are in agreement with the porosity and pore network changes evaluated by capillary absorption, even if the results obtained for the PAASi treatment could appear in**

contradiction with gravimetric test (*i.e.*, a reduction of the water absorbed by capillarity of about 2% and an increase of WC% observed with neutron radiography), However, an accurate inspection of water capillary absorption curves (Figure 2) can simply explain these observations. Indeed, during the first minutes of contact with water, samples treated with PAASi absorbed more water than untreated ones, even if a reduction of the total amount of water was observed at longer time steps.

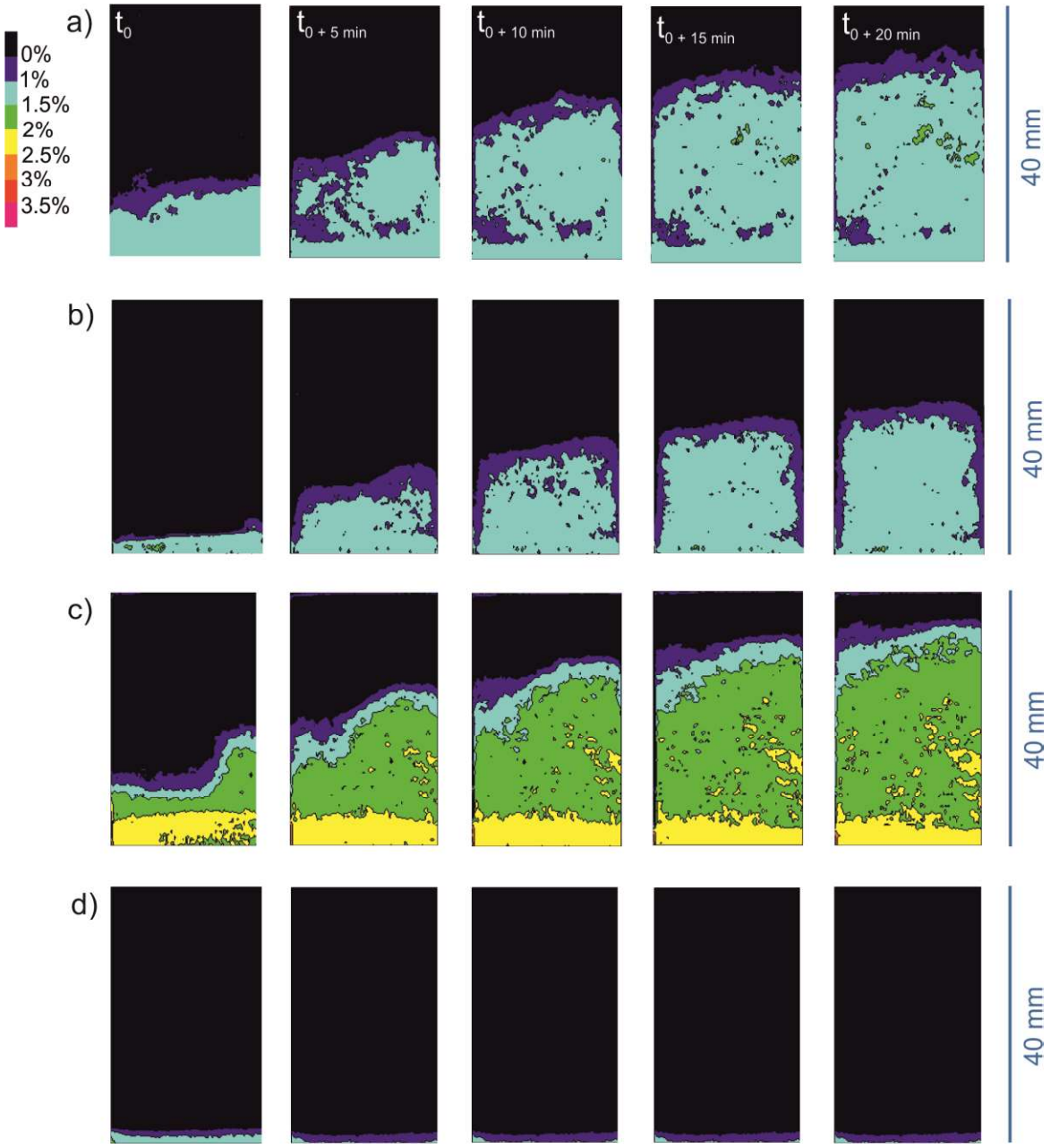

Figure 11. Evolution of the water content during capillary water uptake for (a) untreated samples and samples treated with (b) AlSiX and (c) PAASi consolidants, and (d) hydrophobic product WS3.

3.5 SANS

The Q dependence of the coherent neutron scattered intensity of each untreated and treated sample, I(Q), is depicted in Figure 12. As it was expected for these samples with a high porosity, I(Q) is dominated by the high contrast between pores and solid matter. Because the majority of pores is larger than the inverse of the minimum Q value of the experimental window ($1/Q_{min}$ is of the order of 25 nm), all the scattered intensity is due to the interfaces between solid matter and air in the pores.

The linear dependence of log(I(Q)) vs. log Q is consistent with the fractal formalism that associates roughness to a fractal surface dimension D_S. SANS data **were** fitted by the addition of a power law and a constant:

$$I(Q) = C \cdot Q^{-\alpha} + const$$

with α ranging from −3 to −4. The additive constant is due to the incoherent scattering essentially of hydrogen atoms present in the sample either through the chemical composition of additives or because of hydration water.

Within this simple model, a clear cut interface is associated to the exponent α = 4, and *C* gives the total area of the interface (Porod's law). The scattering due to a rough surface interface can also be described by a power law of the same type: $\alpha = 6-D_S$, with $2<D_s<3$. Obviously, a clear cut surface corresponds to $D_s=2$ while the limit $D_s=3$ corresponds to a mathematically defined interface filling totally the volume.

By analogy, one can associate the roughness to D_s. The larger is D_s and higher is the roughness of the interface. In the matter in question, scattering curves collected on both untreated and treated samples are well described by fractal interfaces. Indeed, a surface fractal law fits the curves in the whole investigated Q range (Q_{min} = 0.0044, Q_{max} = 0.42) with a slope of the different I(Q) ranging from −3 to −4, with variations related to the presence of the products on the pore surfaces.

Essentially, two different slopes are clearly observed, corresponding to values of D_s of the order of either 2.4–2.5 or 2.8 (Table **6**). Certainly, the first describes smoother interfaces, **whereas** the cases where D_s is of the order of 2.8 correspond to a higher roughness of the interfaces.

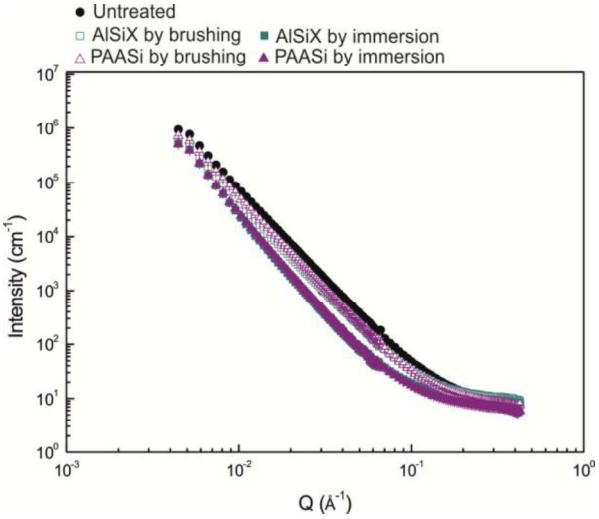

Figure 12. Scattered SANS intensity for untreated sample and samples treated with consolidants (AlSiX and PAASi) by brushing or by immersion.

Thus, starting from a rough surface described by a fractal dimension of 2.8 in **the** untreated stone, the application of the products by immersion clearly penetrated pores, **leading to** a smoothing of the pore surfaces. In contrast, a test with application of the products by brushing **did** not **lead to** relevant changes in **the** small pore-air interfaces, **and** therefore **did** not greatly affect the structural features of the substrate. **To summarize, SANS data clearly indicated that taking advantage from their *nanosize*, the tested products were able to penetrate also pores with a diameter of the order of the inverse of the investigated Q range. Products may occupy the pore surface as a smooth layer of particles. However, differences in surface roughness were only detected when products were applied by immersion, suggesting that this method is preferable because it ensures higher bonding of the product to the pore surface and the complete penetration of consolidants into nano-sized pores.**

It has to be noticed that the roughness changes at the pore-air interfaces shown by the D_s variations can also help to explain the modification of the drying rate due to the presence of products. In this direction, since nanoparticles were mainly located on pore surfaces and not inside the pores, they affected the second stage of the drying rate controlled by vapor diffusion at air-particle interface.

4. Conclusions

In this study, a hybrid patented product constituted by polyamidoamine with siloxane functionality, **named** PAASi, and a hybrid sol based on an Al-Si network functionalized with organic chains, **named** AlSiX, were

tested as consolidants on a calcarenite substrate (named Sabucina stone), alone or associated with the hydrophobic coating WS3 (**based on colloidal silica with fluorinated groups**). **This study aimed at evaluating the compatibility of the studied hybrid products with porous calcareous stones and highlighting the merits of multi-scale laboratory investigation procedure.**

The results showed that the Al-Si-based product is not advisable in material conservation of calcarenites because it led to unacceptable changes. On the contrary, calcarenite substrates could be treated with a polyamidoamine-based product, even if it showed a lower ability to reduce water absorption assuring however acceptable vapor permeability reduction. Some negative aspects and unwanted effects, such as chromatic changes or long-term preservation performances, could be overtaken by exploring alternative application methods and/or curing procedure. Generally, it is possible to argue that treatment by immersion is preferable, because it ensures a complete penetration of consolidants into nano-sized pores, not obtained by brushing. However, the application method could be improved, e.g., by washing the surface, wiping excess product after immersion, testing longer immersion procedures, and/or different curing time. Finally, as regards the combined consolidation and protective application, it has to be carefully evaluated by considering the influence of the hydrophobic coating in the kinetics of drying and in supersaturation equilibria when moisture can go through the hydrophobic barrier (*e.g.*, after the partial removal of product due to weathering and/or the possible discontinuous coating on the substrate), as suggested also by the dramatic reduction of the water vapor permeability. Of course, additional studies will be welcomed in order to **explore the possible ability of this class of hybrid coatings to preserve different kind of substrates, especially** low porous **ones**, **for** which consolidation appears particularly critical.

Going to evaluate the potential of integrating multi-scale methods in consolidation tests, water absorption, mercury intrusion porosimetry, and µCT methods **offered** together an overview on the changes in pore structure of the studied stone in the range 0.007–200 µm after the application of consolidant products. They provided consistent results, even if some discrepancies due to the intrinsic differences among the applied methods have to be considered [67]. **Thus,** the applied approach, and especially the use of imaging and small angle scattering methods allowed to better understand interactions between new products and substrates, supplying quantitative data about pore ranges in which consolidants interact with stone, and

adequately supporting the interpretation of material behavior especially against water. In this direction, the possibility to incorporate standard routines and/or substitute destructive testing with non-destructive ones seems to be a valid alterative to evaluate efficiency and monitor behavior of stones treated with consolidant products.

Acknowledgments

Many thanks to **A. Sutter, A. Rovazzani, and S. Chirico** (**OPA Pisa**) for having **assisted microdrilling tests**.

References

[1] E. Sassoni, G. Graziani, E. Franzoni, An innovative phosphate-based consolidant for limestone. Part 1: Effectiveness and compatibility in comparison with ethyl silicate, Constr. Build. Mater. 102 (2016) 918–930. doi:10.1016/j.conbuildmat.2015.04.026.

[2] J.D. Rodrigues, A. Grossi, E. Franzoni, S. Naidu, S. Naidu, Indicators and ratings for the compatibility assessment of conservation actions, J. Cult. Herit. 8 (2007) 32–43. doi:10.1016/j.culher.2006.04.007.

[3] L. Toniolo, T. Poli, V. Castelvetro, A. Manariti, O. Chiantore, M. Lazzari, Tailoring new fluorinated acrylic copolymers as protective coatings for marble, J. Cult. Herit. 3 (2002) 309–316. doi:10.1016/S1296-2074(02)01240-2.

[4] G. Cappelletti, P. Fermo, Hydrophobic and superhydrophobic coatings for limestone and marble conservation, in: Smart Compos. Coatings Membr., Elsevier, 2016: pp. 421–452. doi:10.1016/B978-1-78242-283-9.00015-4.

[5] S.A. Ruffolo, A. Macchia, M.F. La Russa, L. Mazza, C. Urzì, F. De Leo, M. Barberio, G.M. Crisci, Marine Antifouling for Underwater Archaeological Sites: TiO_2 and Ag-Doped TiO_2, Int. J. Photoenergy. 2013 (2013) 1–6. doi:10.1155/2013/251647.

[6] P. Munafò, G.B. Goffredo, E. Quagliarini, TiO2-based nanocoatings for preserving architectural stone surfaces: An overview, Constr. Build. Mater. 84 (2015) 201–218. doi:10.1016/J.CONBUILDMAT.2015.02.083.

[7] A. Sierra-Fernandez, L.S. Gomez-Villalba, M.E. Rabanal, R. Fort, New nanomaterials for applications in conservation and restoration of stony materials: A review, Mater. Construcción. 67 (2017) 107. doi:10.3989/mc.2017.07616.

[8] E. Zendri, E. Balliana, F.C. Izzo, M.M. Di Crescenzo, L. Falchi, M. Sgobbi, G. Biscontin, The Choise of Parameters for the Monitoring and the Maintenance of Architectural Stone Surfaces, Int. J. Herit. Digit. Era. 1 (2012) 331–335. doi:10.1260/2047-4970.1.0.331.

[9] Delgado, STONE CONSOLIDATION : RESEARCH AND PRACTICE, in: J.D. Rodrigues (Ed.), Int . Symp . Work. Art Conserv. Sci. Today, Thessaloniki , Greece, 2010. https://www.researchgate.net/profile/Jose_Rodrigues23/publication/257919755_Stone_consolidation_Research_and_practice/links/0deec52613c0ec479a000000.pdf.

[10] J.D. Rodrigues, A. Grossi, Indicators and ratings for the compatibility assessment of conservation actions, J. Cult. Herit. 8 (2007) 32–43. doi:10.1016/j.culher.2006.04.007.

[11] V. Cnudde, M. Boone, High-resolution X-ray computed tomography in geosciences: A review of the current technology and applications, Earth-Science Rev. 123 (2013) 1–17. doi:10.1016/J.EARSCIREV.2013.04.003.

[12] E. Perfect, C.L. Cheng, M. Kanga, M.Z. Bilheux, J.. Lamanna, M.J. Gragg, D.M. Wright, Neutron imaging of hydrogen-rich fluids in geomaterials and engineered porous media: A review, Earth-Science Rev. 129 (2014) 120–135. doi:10.1016/J.EARSCIREV.2013.11.012.

[13] B. Masschaele, M. Dierick, V. Cnudde, L. Van Hoorebeke, S. Delputte, A. Gildemeister, R. Gaehler, A. Hillenbach, High-speed thermal neutron tomography for the visualization of water repellents, consolidants and water uptake in sand and lime stones, Radiat. Phys. Chem. 71 (2004) 807–808. doi:10.1016/J.RADPHYSCHEM.2004.04.102.

[14] M. Dierick, J. Vlassenbroeck, B. Masschaele, V. Cnudde, L. Van Hoorebeke, A. Hillenbach, High-speed neutron tomography of dynamic processes, Nucl. Instruments Methods Phys. Res. Sect. A Accel. Spectrometers, Detect. Assoc. Equip. 542 (2005) 296–301. doi:10.1016/J.NIMA.2005.01.152.

[15] V. Cnudde, M. Dierick, J. Vlassenbroeck, B. Masschaele, E. Lehmann, P. Jacobs, L. Van Hoorebeke, Determination of the impregnation depth of siloxanes and ethylsilicates in porous material by neutron radiography, J. Cult. Herit. 8 (2007) 331–338. doi:10.1016/J.CULHER.2007.08.001.

614 [16] V. Cnudde, P. Dubruel, K. De Winne, I. De Witte, B. Masschaele, P. Jacobs, E. Schacht, The use of
615 X-ray tomography in the study of water repellents and consolidants, Eng. Geol. 103 (2009) 84–92.
616 doi:10.1016/J.ENGGEO.2008.06.013.
617 [17] V.G. Ruiz de Argandoña, C. L., A. Rodríguez-Rey, L.M. Suárez del Río, C. Celorio, X-ray Computed
618 Tomography study of the influence of consolidants on the hydric properties of sandstones for stone
619 conservation studies, Eng. Geol. 103 (2009) 69–75. doi:10.1016/J.ENGGEO.2008.06.008.
620 [18] F. Hameed, B. Schillinger, A. Rohatsch, M. Zawisky, H. Rauch, Investigations of stone consolidants
621 by neutron imaging, Nucl. Instruments Methods Phys. Res. Sect. A Accel. Spectrometers, Detect.
622 Assoc. Equip. 605 (2009) 150–153. doi:10.1016/J.NIMA.2009.01.139.
623 [19] M. Slavíková, F. Krejci, J. Zemlicka, M. Pech, P. Kotlík, J. Jakubek, X-ray radiography and
624 tomography for monitoring the penetration depth of consolidants in Opuka – the building stone of
625 Prague monuments, J. Cult. Herit. 13 (2012) 357–364. doi:10.1016/J.CULHER.2012.01.010.
626 [20] B. Sena da Fonseca, S. Piçarra, A.P. Ferreira Pinto, M. de F. Montemor, G. Lucovsky, R.F. Reidy, Z.
627 Xu, A. Murru, A.M.Z. Slawin, E. Tuveri, J.D. Woollins, M. Arca, Development of formulations
628 based on TEOS-dicarboxylic acids for consolidation of carbonate stones, New J. Chem. 40 (2016)
629 7493–7503. doi:10.1039/C6NJ00455E.
630 [21] E. Franzoni, G. Graziani, E. Sassoni, TEOS-based treatments for stone consolidation: acceleration of
631 hydrolysis–condensation reactions by poulticing, J. Sol-Gel Sci. Technol. 74 (2015) 398–405.
632 [22] E. Franzoni, G. Graziani, E. Sassoni, G. Bacilieri, M. Griffa, P. Lura, Solvent-based ethyl silicate for
633 stone consolidation: influence of the application technique on penetration depth, efficacy and pore
634 occlusion, Mater. Struct. 48 (2015) 3503–3515. doi:10.1617/s11527-014-0417-1.
635 [23] D. Pinna, B. Salvadori, S. Porcinai, Evaluation of the application conditions of artificial protection
636 treatments on salt-laden limestones and marble, Constr. Build. Mater. 25 (2011) 2723–2732.
637 doi:10.1016/j.conbuildmat.2010.12.023.
638 [24] A.P.F. Pinto, J.D. Rodrigues, Stone consolidation: The role of treatment procedures, J. Cult. Herit. 9
639 (2008) 38–53. doi:10.1016/j.culher.2007.06.004.
640 [25] E. Franzoni, E. Sassoni, G. Graziani, Brushing, poultice or immersion? The role of the application
641 technique on the performance of a novel hydroxyapatite-based consolidating treatment for limestone,

J. Cult. Herit. 16 (2015) 173–184. doi:10.1016/j.culher.2014.05.009.

[26] A.P. Ferreira Pinto, J. Delgado Rodrigues, Consolidation of carbonate stones: Influence of treatment procedures on the strengthening action of consolidants, J. Cult. Herit. 13 (2012) 154–166. doi:10.1016/j.culher.2011.07.003.

[27] M.L. Tabasso, S. Simon, Testing methods and criteria for the selection/evaluation of products for the conservation of porous building materials, Stud. Conserv. 51 (2006) 67–82. doi:10.1179/sic.2006.51.Supplement-1.67.

[28] C. Salazar-Hernández, J. Cervantes, M.J. Puy-Alquiza, R. Miranda, Conservation of building materials of historic monuments using a hybrid formulation, J. Cult. Herit. 16 (2015) 185–191. doi:10.1016/J.CULHER.2014.05.004.

[29] L. Bergamonti, A. Berzolla, E. Chiappini, E. Feci, L. Maistrello, S. Palanti, G. Predieri, G. Vaccari, Polyamidoamines (PAAs) functionalized with siloxanes as wood preservatives against fungi and insects, Holzforschung. 71 (2017) 445–456. doi:10.1515/hf-2016-0010.

[30] F. Girardi, L. Bergamonti, C. Isca, G. Predieri, C. Graiff, P.P. Lottici, E. Cappelletto, N. Ataollahi, R. Di Maggio, Chemical–physical characterization of ancient paper with functionalized polyamidoamines (PAAs), Cellulose. 24 (2017) 1057–1068. doi:10.1007/s10570-016-1159-8.

[31] C.J. Brinker, G.W. Scherer, Sol-gel science : the physics and chemistry of sol-gel processing, Academic Press, 1990.

[32] G. Kickelbick, ed., Hybrid Materials, Wiley-VCH Verlag GmbH & Co. KGaA, Weinheim, Germany, 2006. doi:10.1002/9783527610495.

[33] Y. Liu, J. Liu, Synthesis of TEOS/PDMS-OH/CTAB composite coating material as a new stone consolidant formulation, Constr. Build. Mater. 122 (2016) 90–94. doi:10.1016/J.CONBUILDMAT.2016.06.069.

[34] C. Esposito Corcione, N. De Simone, M.L. Santarelli, M. Frigione, Protective properties and durability characteristics of experimental and commercial organic coatings for the preservation of porous stone, Prog. Org. Coatings. 103 (2017) 193–203. doi:10.1016/J.PORGCOAT.2016.10.037.

[35] C. Salazar-Hernández, M.J.P. Alquiza, P. Salgado, J. Cervantes, TEOS-colloidal silica-PDMS-OH hybrid formulation used for stone consolidation, Appl. Organomet. Chem. 24 (2010) n/a-n/a.

670 doi:10.1002/aoc.1646.
671 [36] M.J. Mosquera, D.M. de los Santos, T. Rivas, Surfactant-Synthesized Ormosils with Application to
672 Stone Restoration, Langmuir. 26 (2010) 6737–6745. doi:10.1021/la9040979.
673 [37] R. Zárraga, J. Cervantes, C. Salazar-Hernandez, G. Wheeler, Effect of the addition of hydroxyl-
674 terminated polydimethylsiloxane to TEOS-based stone consolidants, J. Cult. Herit. 11 (2010) 138–
675 144. doi:10.1016/J.CULHER.2009.07.002.
676 [38] L. de Ferri, P.P. Lottici, A. Lorenzi, A. Montenero, E. Salvioli-Mariani, Study of silica nanoparticles
677 – polysiloxane hydrophobic treatments for stone-based monument protection, J. Cult. Herit. 12 (2011)
678 356–363. doi:10.1016/J.CULHER.2011.02.006.
679 [39] F. Xu, D. Li, Q. Zhang, H. Zhang, J. Xu, Effects of addition of colloidal silica particles on TEOS-
680 based stone protection using n-octylamine as a catalyst, Prog. Org. Coatings. 75 (2012) 429–434.
681 doi:10.1016/j.porgcoat.2012.07.001.
682 [40] I. Alfieri, A. Lorenzi, L. Ranzenigo, L. Lazzarini, G. Predieri, P.P. Lottici, Synthesis and
683 characterization of photocatalytic hydrophobic hybrid TiO2-SiO2 coatings for building applications,
684 Build. Environ. 111 (2017) 72–79. doi:10.1016/J.BUILDENV.2016.10.019.
685 [41] L. Bergamonti, F. Bondioli, I. Alfieri, S. Alinovi, A. Lorenzi, G. Predieri, P.P. Lottici, Weathering
686 resistance of PMMA/SiO 2 /ZrO 2 hybrid coatings for sandstone conservation, Polym. Degrad. Stab.
687 147 (2018) 274–283. doi:10.1016/j.polymdegradstab.2017.12.012.
688 [42] L. Bergamonti, E. Chiappini, S. Palanti, L. Maistrello, G. Predieri, Wood preservative compositions,
689 WO 2015004590 A1, 2016.
690 [43] A. Bellanca, E. Curcuruto, S. Lo Bue, R. Neri, Petrografia, geochimica e riferimenti all'impiego
691 storico delle calcareniti plioceniche in Sabucina, Sicilia centrale, Miner. Petrogr. Acta. 42 (1993)
692 193–210.
693 [44] G. Barone, P. Mazzoleni, G. Pappalardo, S. Raneri, Microtextural and microstructural influence on
694 the changes of physical and mechanical proprieties related to salts crystallization weathering in
695 natural building stones. The example of Sabucina stone (Sicily), Constr. Build. Mater. 95 (2015).
696 doi:10.1016/j.conbuildmat.2015.07.131.
697 [45] UNI 10921 - Cultural Heritage - Natural And Artificial Stones - Water Repellents - Application On

698 Samples And Determination Of Their Properties In Laboratory, (2001).
699 [46] UNI 11207 - Cultural heritage - natural and artificial stones - Determination of static contact angle on
700 laboratory specimens, (2007).
701 [47] UNI EN 15886, Conservation of cultural property - Test methods - Colour measurement of surfaces,
702 (2010).
703 [48] UNI EN 15801, Determination of water absorption by capillarity immersion, (2010).
704 [49] NORMAL 7/81 Natural stones test methods: Determination of water absorption by total immersion,
705 (n.d.).
706 [50] NORMAL 29/88 Determination of Drying Index, (n.d.).
707 [51] UNI EN 12370, Natural stones test methods: Determination of resistance to salt crystallization,
708 (2001).
709 [52] P.N. Manoudis, A. Tsakalof, I. Karapanagiotis, I. Zuburtikudis, C. Panayiotou, Fabrication of super-
710 hydrophobic surfaces for enhanced stone protection, Surf. Coatings Technol. 203 (2009) 1322–1328.
711 doi:10.1016/J.SURFCOAT.2008.10.041.
712 [53] P.N. Manoudis, I. Karapanagiotis, A. Tsakalof, I. Zuburtikudis, B. Kolinkeová, C. Panayiotou,
713 Superhydrophobic films for the protection of outdoor cultural heritage assets, Appl. Phys. A. 97
714 (2009) 351–360. doi:10.1007/s00339-009-5233-z.
715 [54] J.D. Rodrigues, A.F. Pinto, D.R. da Costa, Tracing of decay profiles and evaluation of stone
716 treatments by means of microdrilling techniques, J. Cult. Herit. 3 (2002) 117–125.
717 doi:10.1016/S1296-2074(02)01172-X.
718 [55] B.C. Masschaele, V. Cnudde, M. Dierick, P. Jacobs, L. Van Hoorebeke, J. Vlassenbroeck, UGCT:
719 New X-ray radiography and tomography facility, Nucl. Instruments Methods Phys. Res. Sect. A
720 Accel. Spectrometers, Detect. Assoc. Equip. 580 (2007) 266–269. doi:10.1016/j.nima.2007.05.099.
721 [56] J. Vlassenbroeck, M. Dierick, B. Masschaele, V. Cnudde, L. VanHoorebeke, P. Jacobs, Software
722 tools for quantification of X-ray microtomography at the UGCT, Nucl. Instruments Methods Phys.
723 Res. Sect. A Accel. Spectrometers, Detect. Assoc. Equip. 580 (2007) 442–445.
724 doi:10.1016/J.NIMA.2007.05.073.
725 [57] L. Brabant, J. Vlassenbroeck, Y. De Witte, V. Cnudde, M.N. Boone, J. Dewanckele, L. Van

726 Hoorebeke, Three-Dimensional Analysis of High-Resolution X-Ray Computed Tomography Data
727 with Morpho+, Microsc. Microanal. 17 (2011) 252–263. doi:10.1017/S1431927610094389.
728 [58] M.D. Abràmoff, P.J. Magalhães, S.J. Ram, Image Processing with ImageJ, Biophotonics Int. 11
729 (2004) 36–42. https://imagescience.org/meijering/publications/download/bio2004.pdf (accessed
730 September 16, 2017).
731 [59] F.H. Kim, D. Penumadu, D.S. Hussey, Water Distribution Variation in Partially Saturated Granular
732 Materials Using Neutron Imaging, J. Geotech. Geoenvironmental Eng. 138 (2012) 147–154.
733 doi:10.1061/(ASCE)GT.1943-5606.0000583.
734 [60] J.R. PHILIP, THE THEORY OF INFILTRATION, Soil Sci. 83 (1957) 345–358.
735 doi:10.1097/00010694-195705000-00002.
736 [61] D. Bale Harold, S. Paul, Small-Angle X-Ray-Scattering Investigation of Submicroscopic Porosity
737 with Fractal Properties, Phys. Rev. Lett. 53 (1984) 596–599.
738 [62] O. García, K. Malaga, Definition of the procedure to determine the suitability and durability of an
739 anti-graffiti product for application on cultural heritage porous materials, J. Cult. Herit. 13 (2012) 77–
740 82. doi:10.1016/J.CULHER.2011.07.004.
741 [63] V. Cnudde, M. Dierick, J. Vlassenbroeck, B. Masschaele, E. Lehmann, P. Jacobs, L. Van Hoorebeke,
742 High-speed neutron radiography for monitoring the water absorption by capillarity in porous
743 materials, Nucl. Instruments Methods Phys. Res. Sect. B Beam Interact. with Mater. Atoms. 266
744 (2008) 155–163. doi:10.1016/j.nimb.2007.10.030.
745 [64] R. Snethlage, Stone Conservation, in: S. Siegesmund, R. Snethlage (Eds.), Stone Archit., Springer
746 Berlin Heidelberg, Berlin, Heidelberg, 2014: pp. 415–550. doi:10.1007/978-3-642-45155-3_7.
747 [65] I. Karapanagiotis, A. Pavlou, P.N. Manoudis, K.E. Aifantis, Water repellent ORMOSIL films for the
748 protection of stone and other materials, Mater. Lett. 131 (2014) 276–279.
749 doi:10.1016/J.MATLET.2014.05.163.
750 [66] S. Raneri, V. Cnudde, T. De Kock, H. Derluyn, G. Barone, P. Mazzoleni, X-ray computed micro-
751 tomography to study the porous structure and degradation processes of a building stone from
752 Sabucina (Sicily), Eur. J. Mineral. 27 (2015). doi:10.1127/ejm/2015/0027-2433.
753 [67] V. Cnudde, A. Cwirzen, B. Masschaele, P.J.S. Jacobs, Porosity and microstructure characterization of

754 building stones and concretes, Eng. Geol. 103 (2008) 76–83.
755 https://research.aalto.fi/en/publications/porosity-and-microstructure-characterization-of-building-
756 stones-and-concretes(26bcc18e-bf24-4baf-8a5a-c4ae9ac863d9)/export.html (accessed September 16,
757 2017).
758
759
760

761 **Tables**

762

763 **Table 1.** Summary of the number, shape, and dimension of the analyzed samples.

Test or experiment	Number of sample	Shape	Dimension	Product location	Standard recommendation
Microscopic analysis	5	Thin section	standard	Around the sample	
Colorimetric test	15 (3 per treatment)	Cubes	4x4x4 cm^3	Top of the sample	UNI EN 15886:2010
Static contact angle	4	Cubes	4x4x4 cm^3	Top of the sample	UNI 11207:2007
Capillary water absorption	15 (3 per treatment)	Cubes	4x4x4 cm^3	Around the sample	UNI EN 15801:2010
Total immersion	75 (15 per treatment)	Cubes	4x4x4 cm^3	Around the sample	NORMAL 7/81
Resistance to salt crystallization	75 (15 per treatment)	Cubes	4x4x4 cm^3	Around the sample	UNI EN 12370:2001
DRMS	5 (1 per treatment, 4 holes)	Cubes	7x7x7 cm^3	Around the sample	
MIP analysis	9 (3 per treatment)	Cubes	1 cm^3	Top of the sample	
X-ray micro-tomography	2 (1 per treatment)	Cylinder	7 mm in diameter	Top of the sample	
Neutron radiography	15 (3 per treatment)	Parallelepiped	2x2x4 cm^3	Around the sample	
SANS	5 (1 per treatment)	Thin slices	< 1 mm thick	Around the sample	

764

765 **Table 2.** Average color difference ΔE^* of untreated samples and samples treated with both consolidants

766 (PAASi and AlSiX) and hydrophobic (WS3) products.

Samples	L^*	a^*	b^*	ΔE^* ($n = 3$)
Untreated	66	5	21	
PAASi	63	7	25	**5**
PAASi + WS3	63	6	24	**4**
AlSiX	56	8	29	**13**
AlSiX + WS3	52	12	30	**18**

767

768 **Table 3.** Physical properties (± standard deviation) of untreated samples and samples treated with both
769 consolidants (PAASi and AlSiX) and hydrophobic (WS3) products. AC is the absorption coefficient, CI is
770 the imbibition coefficient, DI is the drying index, and ΔM is the mass variation after salt crystallization test.

Samples	AC (g cm^{-2} t$^{-0.5}$)[1] (n = 3)	CI (%)[2] (n = 15)	DI (%)[3] (n = 15)	ΔM (%)[4] (n = 15)
Untreated	0.03±0.01	11.5 ± 1.2	0.4	−11.1
PAASi	0.04±0.01	10.8± 0.8	0.7	−6.6
PAASi + WS3	0.02±0.01	11.1± 2.0	0.7	−12.7
AlSiX	0.02±0.01	10.4± 0.4	0.7	−21.8
AlSiX + WS3	0.01±0.01	10.8± 0.5	0.5	−19.5

[1] UNI EN 15801:2010; [2]NORMAL 7/81; [3]NORMAL 29/88; [4]UNI EN 12370:2001

771

772 **Table 4.** Average parameters (± standard deviation) derived from mercury intrusion porosimetry on
773 untreated samples and samples treated with consolidants (AlSiX and PAASi).

Parameters	Untreated (n = 3)	*PAASi* (n = 3)	AlSiX (n = 3)
Total intruded volume (cm^3 g)	0.14± 0.01	0.14 ± 0.02	0.13± 0.01
Bulk density (g cm^{-3})	1.98± 0.05	1.95 ± 0.10	1.98± 0.05
Apparent density (g cm^{-3})	2.71± 0.06	2.67 ± 0.06	2.65± 0.02
Porosity (%)	26.86± 0.94	27.07 ± 3.09	25.44± 1.75
Total surface area (m^2 g)	1.89± 0.20	1.75 ± 0.22	1.17± 0.22
Average pore radius (µm)	0.14± 0.01	0.16 ± 0.04	0.22± 0.02
Modal pore radius (µm)	8.56± 30.9	14.22 ± 5.07	12.55± 2.50
Median pore radius (µm)	2.25± 0.12	2.90 ± 1.30	4.21± 0.45

774

775 **Table 5.** Sorptivity parameter B (± standard deviation) calculated for untreated samples and samples treated
776 with consolidant (AlSiX and PAASi) and hydrophobic (WS3) products.

Samples	Sorptivity parameter B (mm s$^{-0.5}$) (n = 3)
Untreated	0.69 ±0.01
PAASi	0.59 ±0.01
PAASi + WS3	0.00 ± 0.00
AlSiX	0.56 ±0.01
AlSiX + WS3	0.00 ± 0.00

777

778 **Table 6.** Calculated fractal dimension from α exponent for untreated sample and samples treated with
779 consolidants (AlSiX and PAASi) by brushing or by immersion.

Samples	C (cm^{-1})	α	D_s
Untreated	8.5 ± 0.1	−3.1545 ± 0.0003	2.8
PAASi by brushing	6.3 ± 0.1	−3.2239 ± 0.0004	2.8
AlSiX by brushing	9.7 ± 0.1	−3.2396 ± 0.0004	2.8
PAASI by immersion	6.6 ± 0.1	−3.5356 ± 0.0006	2.5
AlSiX by immersion	9.1 ± 0.1	−3.5935 ± 0.0006	2.4

780

Method Details (MethodsX)

Click here to download Method Details (MethodsX): MethodsX-Article_26052018_.doc